Geophysical Research Letters

RESEARCH LETTER
10.1029/2021GL095829

Key Points:

- Radiative forcing in the eastern tropical Pacific leads to an El Niño-like warming pattern due to the absence of strong radiative damping
- Western tropical Pacific is subject to effective radiative damping via shortwave cloud radiative effect and wind-evaporation-sea surface temperature feedback
- Inter-model spread of the future tropical Pacific warming pattern is due to uncertainty in the eastern Pacific ocean heat uptake response

Supporting Information:

Supporting Information may be found in the online version of this article.

Correspondence to:

S. M. Kang,
skang@unist.ac.kr

Citation:

Park, C., Kang, S. M., Stuecker, M. F., & Jin, F.-F. (2022). Distinct surface warming response over the western and eastern equatorial Pacific to radiative forcing. *Geophysical Research Letters*, *49*, e2021GL095829. https://doi.org/10.1029/2021GL095829

Received 21 AUG 2021
Accepted 6 JAN 2022

Distinct Surface Warming Response Over the Western and Eastern Equatorial Pacific to Radiative Forcing

Chanyoung Park[1], Sarah M. Kang[1], Malte F. Stuecker[2], and Fei-Fei Jin[3]

[1]Department of Urban and Environmental Engineering, Ulsan National Institute of Science and Technology, Ulsan, South Korea, [2]Department of Oceanography and International Pacific Research Center, School of Ocean and Earth Science and Technology, University of Hawai'i at Mānoa, Honolulu, HI, USA, [3]Department of Atmospheric Sciences, School of Ocean and Earth Science and Technology, University of Hawai'i at Mānoa, Honolulu, HI, USA

Abstract This study examines regional characteristics of atmospheric and oceanic feedback processes in the western and eastern equatorial Pacific, by applying a localized surface heating in the respective region in a hierarchy of climate models. A western Pacific forcing is largely offset by a negative shortwave cloud radiative effect and damping via wind-evaporation-SST feedback. In contrast, an eastern Pacific forcing, while being partially compensated for by ocean dynamical adjustments, induces an amplified warming extending to the central Pacific due to weak local damping mechanisms. As for the inter-model spread of the future tropical Pacific surface warming pattern, the ocean heat uptake response in the east can explain much of the spread both on fast (<5 years) and slow (>100 years) timescales. Our results suggest that an "El Niño-like" warming pattern is probable in response to increasing greenhouse gases owing to the strong negative feedback intrinsic to the western Pacific.

Plain Language Summary It is of question whether Earth's surface warming in response to increasing greenhouse gas concentrations will be more amplified in the western (La Niña-like) or eastern (El Niño-like) part of the equatorial Pacific. This response is uncertain across climate models since multiple atmospheric and oceanic feedbacks operate in combination with their relative importance varying in time. We thus prescribe radiative heating either to the western or to the eastern tropical Pacific in a hierarchy of climate model simulations, varying in the degree of atmosphere-ocean coupling, in order to systematically examine different feedback mechanisms at work in the two regions, respectively. Our hierarchical model experiments reveal that strong negative atmospheric feedback mechanisms are intrinsic to the western Pacific while atmospheric feedbacks are less effective in the eastern Pacific with a partially offsetting effect from climatological oceanic upwelling. Therefore, the surface warming is likely to be amplified in the eastern rather than the western equatorial Pacific under uniform radiative heating. In addition, we invoke similar mechanisms to explain the inter-model spread of the future tropical Pacific surface warming pattern, in which uncertainty in ocean dynamical processes turns out to be important on both fast and slow timescales.

1. Introduction

Historical and projected future changes of the tropical Pacific sea surface temperature (SST) mean state have profound impacts on the global climate system. For example, the tropical SST pattern determines regional precipitation distributions following a warmer-get-wetter mechanism (Grose et al., 2014; Kent et al., 2015; Xie et al., 2010). The large-scale atmospheric circulations in the tropics (i.e., Hadley and Walker circulations) are also closely tied to the spatial patterns of tropical SSTs (Ma & Xie, 2013; Yun et al., 2021). Furthermore, variations in tropical Pacific SSTs modulate the location and strength of atmospheric convective activity and hence have far-reaching effects on the extratropical climate through atmospheric Rossby wave propagation (e.g., Trenberth et al., 1998). The tropical Pacific SST pattern also controls the strength of radiative feedbacks (Andrews & Webb, 2018; Armour et al., 2013; Barsugli et al., 2006; Loeb et al., 2020; Senior & Mitchell, 2000), thereby regulating the global-mean surface temperature rise in response to increasing greenhouse gases (GHGs; Kosaka & Xie, 2013).

Despite its widely documented impacts on the global climate, how the tropical Pacific SST pattern may respond to rising GHGs has been debated for decades (e.g., Knutson & Manabe, 1995; DiNezio et al., 2009; Xie et al., 2010; Stuecker, 2021). Several mechanisms involving a dynamic ocean response are proposed to explain

changes in the zonal gradient of equatorial Pacific SST. Clement et al. (1996) suggest that the equatorial zonal SST gradient will increase in response to GHG-induced warming associated with continual upwelling of cold water in the eastern equatorial Pacific, known as the ocean dynamical thermostat mechanism. Another proposed mechanism in favor of the La Niña-like response involves a potential reduction of El Niño-Southern Oscillation (ENSO) SST skewness due to a strengthened thermal upper-ocean stratification in response to GHG forcing (Kohyama et al., 2017). In contrast, positive SST anomalies in the subtropical subduction region can reach the tropics following the shallow subtropical cells and rise in the eastern equatorial Pacific. This oceanic tunnel suggests a reduced equatorial Pacific zonal SST gradient from GHG forcing (Burls et al., 2017; McCreary & Lu, 1994). In addition, a potential weakening of the subtropical cells due to changes in meridional SST gradients and related surface winds would also result in a reduced equatorial Pacific zonal SST gradient (e.g., Stuecker et al., 2020).

Other mechanisms involving atmospheric processes suggest a weakened zonal SST gradient in the equatorial Pacific. The western and eastern tropical Pacific feature distinct evaporative damping efficiencies (Knutson & Manabe, 1995; Xie et al., 2010). The mean evaporation is considerably weaker in the eastern compared to the western tropical Pacific, due to the climatologically lower SST and weaker winds. Hence, a spatially uniform GHG forcing would induce an SST warming that is more enhanced in the eastern compared to the western tropical Pacific. Another factor contributing to a reduced equatorial zonal SST gradient is the distinct shortwave cloud radiative feedback in the two regions (Meehl & Washington, 1996). A surface warming in the western tropical Pacific strengthens deep convection, increasing deep cloud cover, and thereby reduces solar radiation reaching the surface. In contrast, a surface warming in the eastern tropical Pacific decreases lower-atmospheric static stability, causing a reduction in low cloud amount and increased solar radiation reaching the surface.

All these mechanisms contribute to shaping the spatial pattern of tropical Pacific warming but they operate on various time scales (Heede et al., 2020; Heede & Fedorov, 2021). The ocean thermostat mechanism, for example, might be at work in the initial adjustment period to increased radiative forcing but becomes less important with time. This complex interplay among various mechanisms operating on different time scales is partly responsible for a large inter-model uncertainty in projections of the tropical Pacific warming pattern. Constraining the tropical Pacific warming pattern is further complicated by pantropical interbasin climate interactions (Cai et al., 2019) as well as extratropics-to-tropics teleconnection (Kang et al., 2020; Stuecker et al., 2020; X. Zhang et al., 2021). One way to quantify the local and remote contributions to SST warming in the western and eastern tropical Pacific is via Green's function experiments performed with a CAM5 slab ocean model (Figure S1 in Supporting Information S1; Liu et al., 2018). On average, the western Pacific warms by 2.27 K PW^{-1} in response to a local Q-flux forcing while a remote Q-flux forcing warms the region by 1.15 K PW^{-1}. In contrast, the local Q-flux contribution to eastern Pacific warming is 4.83 K PW^{-1} while the remote contribution amounts to 1.33 K PW^{-1}. This suggests that the warming efficiency contrast in the two regions largely arises from their difference in the response to local forcing rather than remote forcing. Thus, this study aims to systematically examine the factors controlling the surface warming extent to local forcing over the western and eastern tropical Pacific using a hierarchy of model experiments, ranging from a fixed SST configuration to a slab ocean model to a full dynamical ocean model. This will offer a better understanding of distinct surface warming pattern changes in response to global warming.

2. Methodology

We use different versions of the NOAA GFDL Climate Model for our hierarchical modeling experiments. The GFDL Atmospheric Model version 2.0 (AM2.0; Anderson et al., 2004) is used with either fixed SSTs (denoted FSST) or coupled to a slab ocean model (denoted SOM). For a fully coupled configuration, the GFDL Climate Model version 2.1 (CM2.1; Delworth et al., 2006) is used, in which AM2.1 is coupled to the Modular Ocean Model version 4 (MOM4). This configuration with a dynamic ocean model is denoted DOM. The atmospheric model has 2° latitude × 2.5° longitude resolution with 24 vertical levels and the ocean model uses 1° latitude × 1° longitude resolution with 50 vertical layers.

We simulate the control climate in FSST by prescribing the SSTs and sea ice concentration to their monthly climatologies (i.e., year 1251–1300 average) of the pre-industrial DOM integration. This FSST control experiment is perturbed by prescribing anomalous SST of +2 K in the western and eastern tropical Pacific, respectively

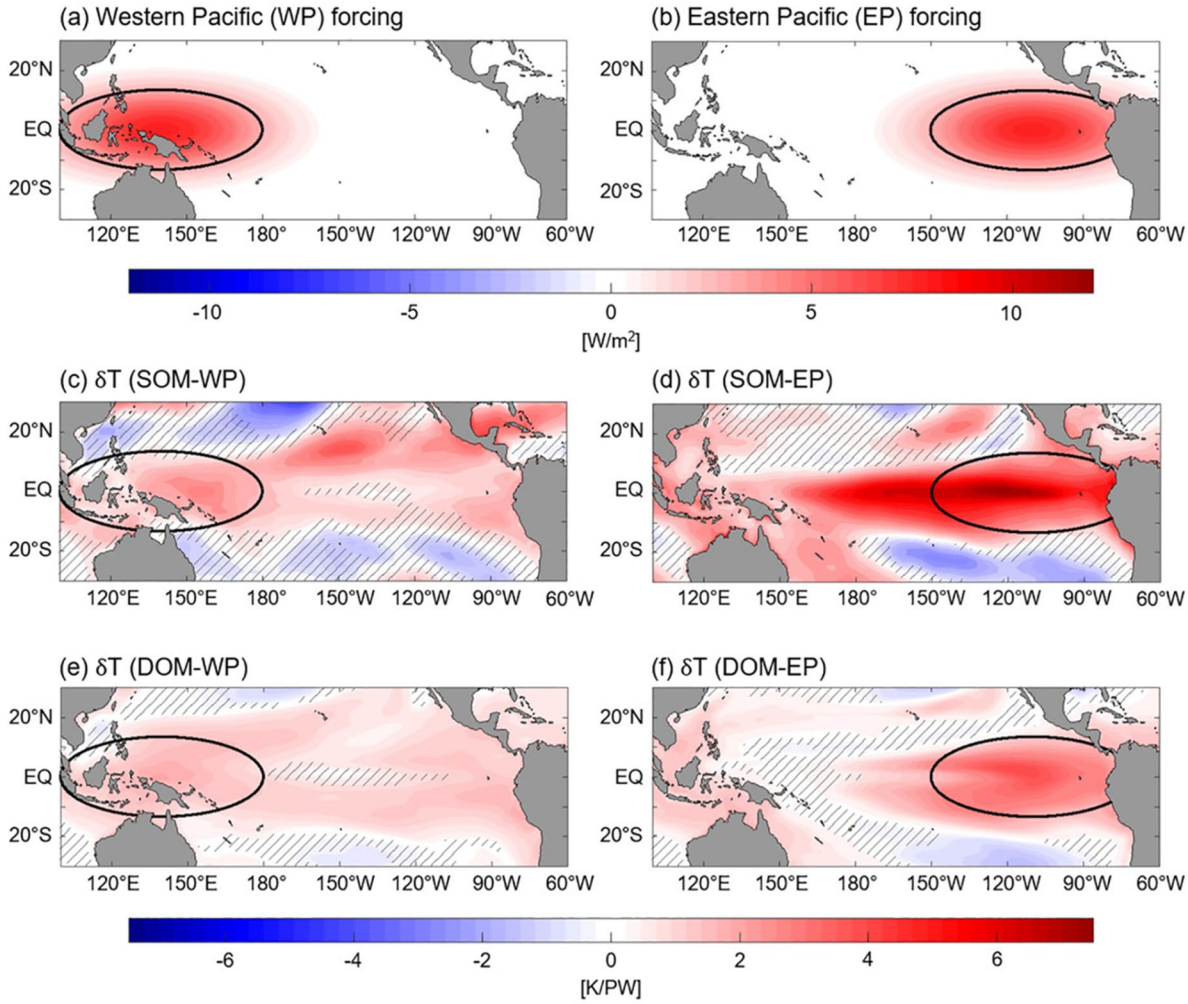

Figure 1. Prescribed sea surface temperature (SST) perturbation in the fixed SST experiments (black contours) and the Q-flux forcing in the slab ocean model (SOM) experiments (red shading) over (a) the western Pacific (WP) or (b) eastern Pacific (EP). The SST response normalized by the Q-flux forcing (PW) in the (c) SOM-WP, (d) SOM-EP, (e) dynamic ocean model (DOM)-WP, and (f) DOM-EP experiments. The ensemble-mean response is shown for the DOM experiments. The black contour defines the local region of either the WP or EP. The regions where the response is not statistically different from zero at the 95% confidence level using a two-tailed *t*-test are hatched.

(black contours in Figures 1a and 1b). Both the control and perturbed experiments are run for 60 years, with the last 30 years used for analysis.

The control climate in SOM is forced by the monthly Q-flux derived from the last 50-year average of a 60-year integration of the FSST control experiment. The SOM control experiment is run for 60 years and the last 30-year average is used for analysis. The SOM perturbation experiments are run with a Gaussian-type Q-flux forcing, either in the western or eastern tropical Pacific, added to the control Q-flux (red shading in Figures 1a and 1b). The Q-flux perturbation amounts to 0.14 PW, with a maximum amplitude of 8 W m^{-2} (the approximate radiative forcing corresponding to a quadrupling of CO_2 concentrations). The SOM perturbation experiments are extended from the SOM control run and are integrated for 50 years with a spin-up period of 20 years.

The DOM control experiment, initialized from year 1241 of a fully spun-up pre-industrial control integration, is run for 60 years and the last 50 years are used for analysis. The DOM control climate is perturbed by a specified heating applied downward at the ocean-atmosphere interface in the same localized regions as in the SOM perturbation experiments, but with a magnitude three times stronger than the Q-flux perturbation in SOM to compensate for the oceanic damping effect. Five ensemble members are integrated for 60 years and the last 50 years are used for analysis. The climate response to either SST or Q-flux perturbation is denoted as δ.

To justify the use of Q-flux instead of a CO_2 perturbation, we compare the normalized SST response to a CO_2 increase and that to a globally uniform Q-flux forcing in the SOM and DOM configurations (Figure S2 in Supporting Information S1). The SST response pattern to a globally uniform Q-flux forcing is in good agreement with that to the increase in CO_2 concentration: over the tropical Pacific (10°S-10°N and 100°E-60°W), the spatial correlation coefficient amounts to 0.78 and 0.87 respectively in SOM and DOM. Moreover, the vertical profile of the temperature response in the equatorial Pacific is largely independent of the nature of forcing (Figure S3 in Supporting Information S1). This implies that our Q-flux perturbation experiments can be used to understand the CO_2-driven SST pattern change in the tropical Pacific. Moreover, to address the robustness of the results, the FSST and SOM experiments are repeated with the NCAR's Community Atmosphere Model version 4.0 (CAM4; Neale et al., 2013). The results are qualitatively similar and here we only show the GFDL model results in the main text for simplicity and the CAM4 results in Supporting Information S1.

We evaluate how our idealized model experimental results can be applied to explaining the multi-model spread of the tropical Pacific warming pattern across 21 CMIP5 and 25 CMIP6 simulations. We analyze the difference between the abrupt CO_2 quadrupling integration and the last 200-year average of the pre-industrial integration. The initial response in the first 5 years is expected to emphasize the effect of regional radiative forcing while the average response over years 131–150 would include the remote effect. To consider a quasi-equilibrated ocean state, we also analyze the response averaged over years 801–1000 after an abrupt CO_2 quadrupling using seven LongRunMIP models (Rugenstein et al., 2019).

3. Results

3.1. Fixed SST Experiments

The FSST experiments with the same SST warm anomaly prescribed in either the western or the eastern tropical Pacific (Figure 2a) clearly reveal the distinct warming efficiency in the two regions. The net surface energy flux response in FSST implies the external forcing required to balance the prescribed SST anomaly. The western Pacific requires 55.11 W m^{-2} to balance a local warming of 1 K whereas only 18.77 W m^{-2} is needed to balance an eastern tropical Pacific SST anomaly (Figure 2b). A similar sensitivity can be found in CAM5.3 of Zhou et al. (2017), with 73.15 W m^{-2} K^{-1} for the western and 31.54 W m^{-2} K^{-1} for the eastern tropical Pacific, respectively. This implies that the western Pacific is subject to a local radiative damping that is at least twice as strong as that in the eastern Pacific.

A surface energy budget decomposition suggests that the shortwave cloud radiative effect at the surface (SWCRE) is one of the major damping mechanisms in the western Pacific (Figure 2c). Based on the Webb et al. (2006) method, the SWCRE-induced cooling mostly results from an increase in non-low clouds (Figure S4a in Supporting Information S1) due to enhanced vertical motion (Figure 2e). This is consistent with previous studies showing that the shortwave radiation in the western tropical Pacific is regulated by high cloud changes (DiNezio et al., 2009; Ramanathan & Collins, 1991). The prescribed warming over the western Pacific is further compensated by a latent heat flux increase in association with enhanced surface wind speed (LH_{wind}; Figure 2d) as a result of low-level wind convergence toward the forcing region. As opposed to the effective negative feedbacks operating in the western Pacific, a local radiative damping effect is very weak in the eastern Pacific (Figure 2b). Instead, a remote impact from the eastern Pacific warm anomaly can be identified in the central Pacific where the latent heat flux decreases due to reduced easterlies (Figure 2d).

3.2. Slab Ocean Model Experiments

Now we proceed to examine if the western and eastern tropical Pacific respond in a distinct manner to the same prescribed Q-flux forcing (Figure 2g) in the SOM configuration to focus on the atmospheric processes separate from ocean dynamics. The SST responses for the western and eastern Pacific Q-flux forcing are respectively shown in Figures 1c and 1d (denoted as SOM-WP and SOM-EP). Despite a prescribed forcing of the same magnitude, the surface warming pattern exhibits a considerable dependence on the geographical location of the forcing. In SOM-WP, the local SST response is relatively weak, which amounts to 1.5 K PW^{-1}, and the SST response outside the western Pacific forcing region is only modest (Figure 1c). In contrast, in SOM-EP, local SSTs increase by 4.3 K PW^{-1}, an increase about three times as large as that in SOM-WP. The warming pattern extends far into the western Pacific with decreasing amplitude, indicative of an El Niño-like warming pattern (Figure 1d).

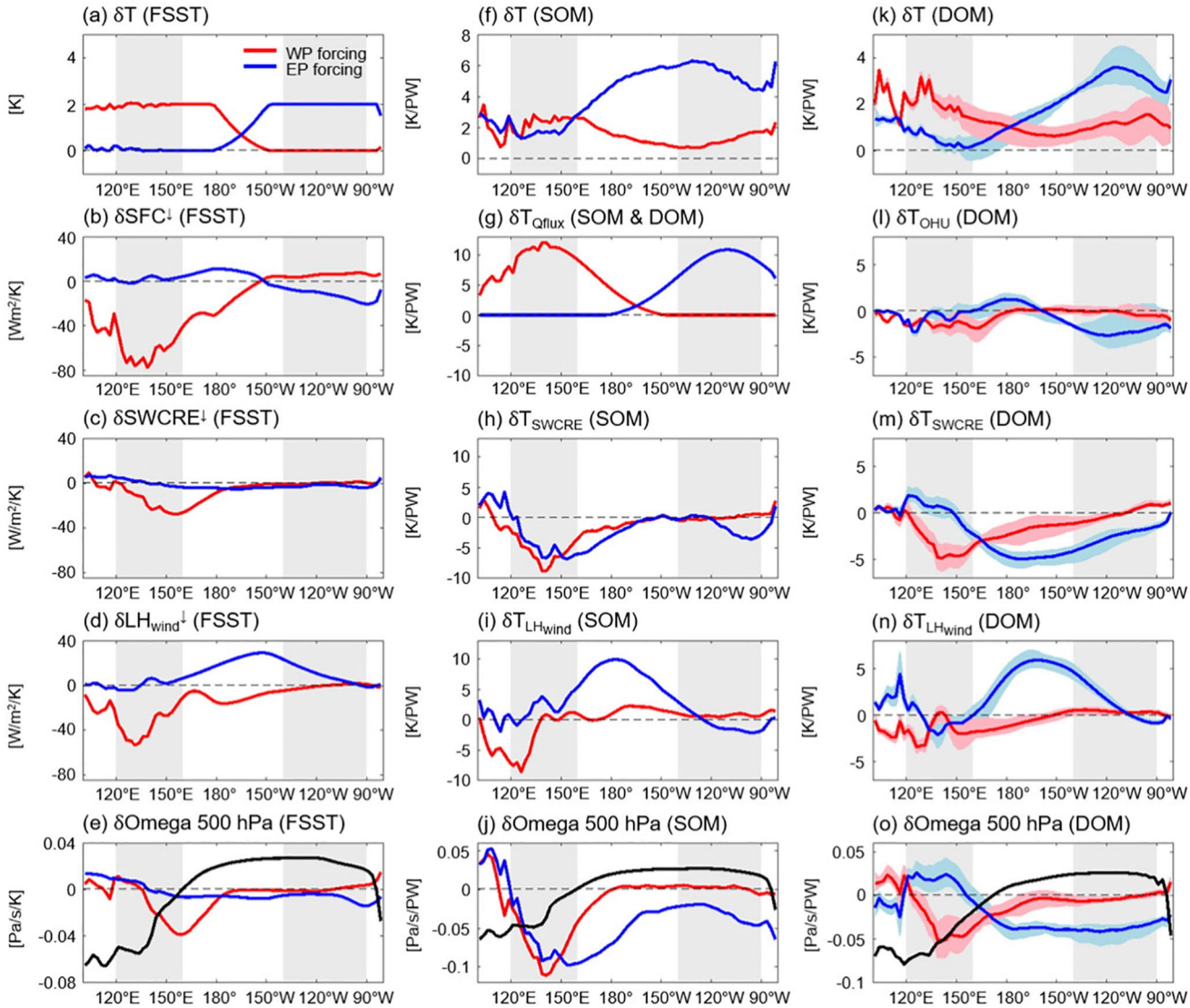

Figure 2. (a) Prescribed sea surface temperature (SST) perturbation, (b) net surface heat flux response (δ SFC; downward positive), (c) δ shortwave cloud radiative effect (SWCRE) (downward positive), and (d) δLH_{wind} (downward positive) across the equatorial (5°S–5°N averaged) Pacific in the fixed SST experiments. The equatorial Pacific (f) δT and the contribution to δT by (g) the prescribed Q-flux, (h) δSWCRE, and (i) δLH_{wind} in the slab ocean model configuration. The equatorial Pacific (k) δT and the contribution to δT by (l) ocean heat uptake response, (m) δSWCRE, and (n) δLH_{wind} in the dynamic ocean model configuration with the ensemble spread in shading. The last row (e, j, o) shows the vertical pressure velocity response at 500 hPa, with the black line denoting the climatology (Pa/s), in the respective model configuration. Panel (b–e) are normalized by the prescribed SST (K) and (f–o) are normalized by the Q-flux perturbation (PW). The response to western Pacific (WP) forcing is shown in red and that to eastern Pacific (EP) forcing in blue. The regions defined as the WP and EP are indicated by gray shading. Please see Supporting Information S1 for details.

Hence, the zonal west-to-east SST gradient across the equatorial Pacific in SOM-WP slightly increases while it substantially decreases in SOM-EP (Figure 2f). To understand the SST pattern formation mechanism, we next perform an energy budget analysis of the mixed layer ocean based on Xie et al. (2010) and L. Zhang and Li (2014) (Figure S5 in Supporting Information S1).

In SOM-WP, the prescribed Q-flux warming is damped by a strongly negative δSWCRE (Figure 2h) associated with non-low cloud changes (Figure S4b in Supporting Information S1) and the wind-induced latent heat flux response (Figure 2i), consistent with the FSST results. By contrast, SOM-EP exhibits no major surface heat flux component offsetting the imposed Q-flux forcing, leading to a pronounced local warming in the eastern Pacific (Figures 1d and 2f). The resultant weakening of surface easterlies along the equatorial Pacific (due to the atmospheric component of the Bjerknes feedback) results in a warming of the central Pacific via reduced latent heat

fluxes (Figure 2i). Consequently, the western Pacific deep convection strengthens and extends eastward, indicated by anomalous ascent to the west of the dateline (Figure 2j), reminiscent of the atmospheric response during an El Niño event (e.g., Bayr et al., 2014). Stronger ascent over the western Pacific is accompanied by a negative δSWCRE (Figure 2h). This, together with the strong local warming in SOM-EP, acts to substantially damp the zonal contrast in the equatorial Pacific SST (Figure 2f).

3.3. Dynamic Ocean Model Experiments

Next, we examine the effect of ocean dynamics on the tropical Pacific SST warming pattern formation. The response to our regional forcing can be regarded as an initial response to a global GHG increase before any remote impacts substantiate. The DOM experiments (Figures 1e and 1f; denoted as DOM-WP and DOM-EP) show the SST spatial warming structure similar to the SOM experiments (Figures 1c and 1d). The response to the WP forcing is particularly similar in the SOM and DOM configurations, with regard to both spatial pattern and amplitude, with a local warming of 1.3 K PW^{-1} in DOM and 1.5 K PW^{-1} in SOM (Figure 1c vs. 1e). By contrast, the oceanic damping effect is evident in the response to the EP forcing, with a local warming of 2.7 K PW^{-1} in DOM as opposed to 4.3 K PW^{-1} in SOM (Figure 1d vs. 1f). The DOM configuration shows the same contrast between the WP and EP experiments as in the SOM configuration albeit weaker, with the local SST response in DOM-EP being twice as large as that in DOM-WP. As a consequence, DOM-EP features a marked El Niño-like warming pattern similar to SOM-EP.

The effect of the ocean heat uptake response (δOHU), which is the sum of net downward surface heat fluxes and prescribed Q-flux, is negligible in DOM-WP (Figure 2l). As a result, the climate response in DOM-WP is very similar to FSST-WP and SOM-WP such that the SWCRE-driven cooling (Figure 2m) and the wind-induced latent heat flux changes (Figure 2n) serve as local damping mechanisms associated with enhanced deep convection over the western Pacific (Figure 2o). By contrast, in DOM-EP, ocean dynamical adjustments act to partially compensate the imposed Q-flux forcing (Figure 2l). The ocean dynamical thermostat (Clement et al., 1996) among other mechanisms could play a role but a detailed ocean heat budget analysis is beyond the scope of this paper. Although the ocean heat uptake effect dampens the imposed Q-flux forcing over the eastern Pacific, the zonal SST gradient in DOM-EP substantially decreases in the equatorial Pacific as opposed to a fairly flat SST response in DOM-WP (Figure 2k). The enhanced warming in the central Pacific in DOM-EP is driven by the wind-induced latent heat flux reduction (Figure 2n), as in SOM-EP (Figure 2i), but is partly offset by the SWCRE cooling (Figure 2m) resulting from a weakening of the Walker circulation (Figure 2o). Note that the peak of SWCRE cooling in DOM-EP (Figure 2m) is shifted eastward into the central Pacific relative to that in SOM-EP (Figure 2h) associated with the distinct Walker circulation response. The Walker circulation weakens in DOM-EP (Figure 2o) while the deep convective activity expands eastward in SOM-EP (Figure 2j) as a substantial surface warming intrudes toward the central Pacific (Figure 1d).

3.4. CMIP5/6 Analysis

The regional forcing experiments explored in the previous sections clearly demonstrate that the eastern equatorial Pacific is more susceptible to prescribed warming than the western equatorial Pacific where effective atmospheric damping mechanisms are at play. The results suggest that a more pronounced warming in the eastern than the western Pacific is expected from an increase in GHG emissions when disregarding any remote impacts. In this section, we evaluate how our results can be applied to explaining the inter-model spread of the zonal SST gradient response to a CO_2 quadrupling across CMIP5/6 models (Figure 3). The initial 5-year average response is examined before the development of pronounced remote impacts to make better connections to our regional warming experiments. We note that consistent results are obtained even for initial 10-year or 20-year average responses. The zonal SST gradient response in the equatorial Pacific is measured by the difference of the SST response between 140°W–90°W and 120°E–160°E (gray shading in Figure 3a) over 5°S–5°N, denoted as ΔEW. A positive ΔEW, corresponding to an El Niño-like warming pattern, implies a reduced zonal SST gradient across the equatorial Pacific. Conversely, a negative ΔEW, corresponding to a La Niña-like warming pattern, implies an enhanced zonal SST gradient across the equatorial Pacific. The inter-model regression of the SST response onto ΔEW (black line in Figure 3a) indicates that the inter-model spread of ΔEW mainly arises from the inter-model spread in the eastern equatorial Pacific SST response. Indeed, ΔEW and the eastern Pacific SST response are

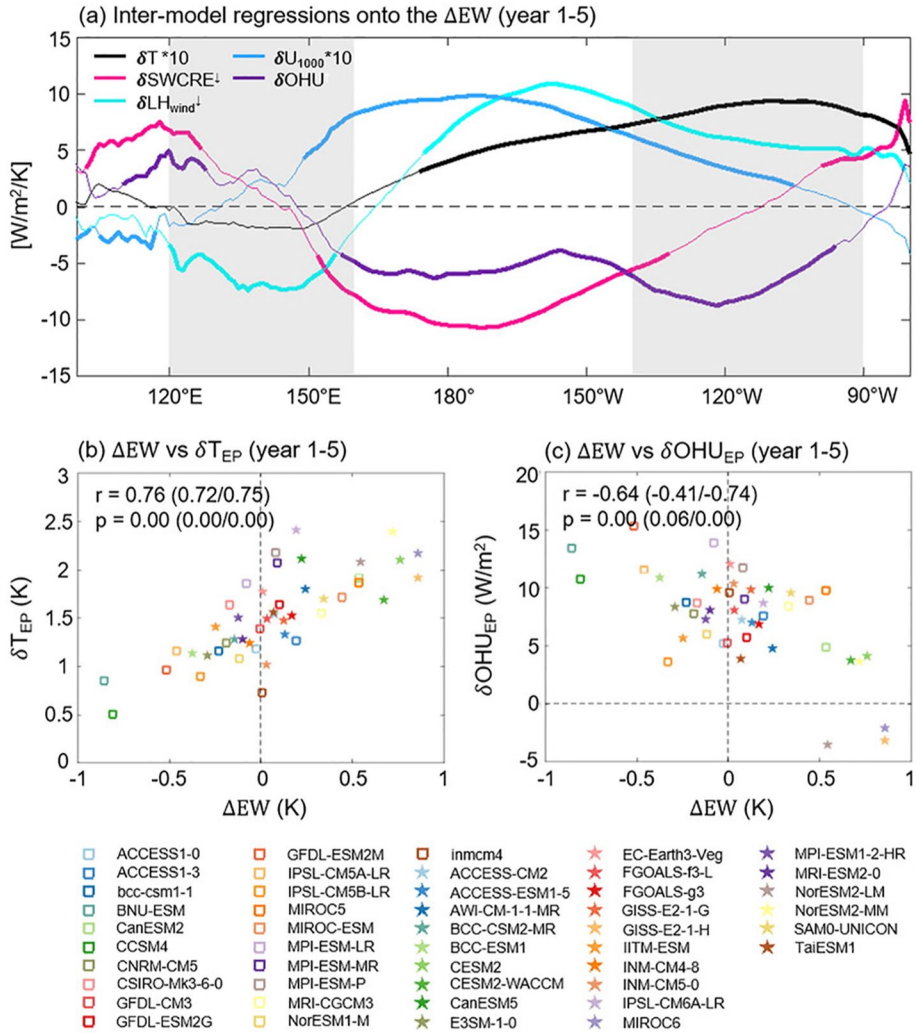

Figure 3. (a) Inter-model regression of δT (black), δshortwave cloud radiative effect (magenta), δLH_{wind} (cyan), the zonal wind response at 1,000 hPa (δU_{1000}; blue), and δOHU (purple) onto ΔEW across the equatorial Pacific averaged over 5°S–E5°N. In the 46 CMIP5/6 models, the initial 5-year average response to abrupt4xCO2 is employed in the analysis. The regression lines for δT (K/K) and δU_{1000} (m/s/K) are scaled by a factor of 10 to facilitate comparison with the heat flux components. Fewer models are used to calculate δLH_{wind} (41 models) due to data availability. The western and eastern equatorial Pacific regions used for ΔEW are shaded in gray. Statistically significant responses according to a two-tailed *t*-test at the 95% confidence level are displayed in bold lines. The scatter plot shows the relationship of ΔEW and projected changes in the eastern equatorial Pacific (5°S–5°N; 140°W–90°W) (b) sea surface temperature and (c) ocean heat uptake (i.e., net downward surface heat flux). Squares represent 21 CMIP5 models and stars represent 25 CMIP6 models. The inter-model correlation coefficient and its p-value are noted in the upper left corner of each panel. Values in parentheses indicate the respective correlation coefficients and p-value for CMIP5 and CMIP6 models only.

highly correlated at 0.76 (p-value = 0.00; Figure 3b), while the western Pacific SST response is poorly correlated with ΔEW at −0.18 (p-value = 0.24; Figure S6a in Supporting Information S1).

Surface heat flux components averaged over 5°S–5°N regressed onto ΔEW are overlaid in Figure 3a. Models with a larger ΔEW are associated with a larger weakening of the Walker circulation, inferred from weaker easterlies along the equatorial Pacific (blue line in Figure 3a). As a consequence, the latent heat flux decreases from the central to eastern Pacific (cyan line) while the SWCRE cooling increases over the central Pacific (magenta line), consistent with DOM-EP (Figures 2m and 2n). The warming driven by the wind-induced latent heat flux reduction is largely offset by the SWCRE-driven cooling (Figure 3a). The δOHU is positive over the eastern Pacific in the majority of models (Figure 3c). Given that a positive δOHU is indicative of anomalous ocean heat divergence, dynamic ocean adjustments act to cool the eastern Pacific in most models, which agrees well with

DOM-EP (Figure 2l). This OHU-induced eastern Pacific cooling is smaller for models with a larger ΔEW, with the two indices anti-correlated at 0.64 (Figures 3a and 3c). Given the close cancellation between the SWCRE and latent heat flux changes, uncertainty in ocean dynamical processes becomes important for explaining the inter-model spread of the projected zonal SST gradient changes in the equatorial Pacific.

4. Summary and Discussion

This study investigates the factors that control the zonal SST gradient across the equatorial Pacific. Using a hierarchy of GFDL models, we reveal distinct surface warming responses in the western and eastern tropical Pacific responding to localized SST and Q-flux perturbations. The western Pacific heating is effectively damped by strong negative atmospheric feedback mechanisms intrinsic to the region. In contrast, the eastern Pacific heating induces a pronounced surface warming due to less effective atmospheric feedbacks with a partially offsetting effect from ocean dynamical adjustments. We performed similar experiments using CAM4 that show consistent results (Figure S7 in Supporting Information S1).

We additionally repeat the FSST and SOM experiments with the bias corrected AM2.0, since the cold tongue bias in climate models has been suggested to be responsible for a reduced zonal SST gradient to GHGs increase (Seager et al., 2019). Specifically, the control FSST experiment is integrated with the observed monthly SST distribution and sea ice concentration over the period between 1982 and 2000 from the National Centers for Environmental Prediction (NCEP) reanalysis (Kalnay et al., 1996). This FSST with the observed mean state is used to derive the Q-flux to construct the bias-corrected SOM, in which one can confirm that the cold tongue bias in the tropical Pacific is clearly removed (Figure S8 in Supporting Information S1). The bias-corrected SOM is then forced with the same Q-flux perturbations as described in Section 2. Even in the absence of the cold tongue bias, the eastern equatorial Pacific warms more effectively than the western equatorial Pacific, confirming the robustness of our results (Figure S9 in Supporting Information S1).

Even though local forcing dominates the local SST response over the western and eastern tropical Pacific (e.g., Figure S1 in Supporting Information S1), we cannot entirely neglect remote effects from extratropics-to-tropics teleconnections, as suggested in previous studies (Burls et al., 2017; England et al., 2020; Heede et al., 2020; Mechoso et al., 2016; Stuecker et al., 2020). During the transient warming period that will potentially dominate the response of the tropical climate system in the near future, a delayed Southern Ocean warming (Armour et al., 2013; Bitz et al., 2006) could cause cooling in the eastern Pacific, creating a La Niña-like pattern (Hwang et al., 2017; Kang et al., 2019, 2020). By contrast, in the slow response, after ∼60 years when the oceanic pathway allows for the extratropical signal to influence the tropics (Fedorov et al., 2015; Thomas & Fedorov, 2017), enhanced extratropical oceanic warming could further contribute to the SST increase over the eastern equatorial Pacific, creating an El Niño-like warming pattern. Thus, the fraction of models that exhibit El Niño-like warming pattern progressively increases with the integration period length, from 59% for the initial 1–5 years (Figures 3b and 3c) to 98% for years 131–150 when local and remote effects are fully involved in the tropical Pacific surface warming pattern (Figures S10b and S10c in Supporting Information S1).

However, with regard to the inter-model spread, we find similar results irrespective of the choice of time period. The inter-model regression of the response of SST and surface flux components onto the ΔEW is similar between the years 1–5 averaged response (Figure 3a) and the years 131–150 averaged response (Figure S10a in Supporting Information S1). As in the initial period, the inter-model spread of a longer-term ΔEW is explained by the eastern Pacific SST response with a statistically significant correlation coefficient of 0.68 (Figure S10b in Supporting Information S1; with zero p-value), and not by the western Pacific SST response ($r = 0.23$, p-value = 0.13; Figure S6b in Supporting Information S1). In addition, the inter-model spread of anomalous OHU in the eastern equatorial Pacific determines a fraction of the model spread in simulated zonal SST contrasts with a correlation coefficient of −0.53 (Figure S10c in Supporting Information S1). Consistent results are obtained on a very slow timescale, as indicated by the average response over years 801–1000 from the LongRunMIP data despite a relatively high p-value of 0.11 due to the small number of models (Figures S10b and S10c in Supporting Information S1). This implies that for both the fast and slow response to an abrupt CO_2 quadrupling, the inter-model spread in the tropical Pacific surface warming patterns originates from uncertainties in the eastern equatorial Pacific SST and OHU responses.

Our findings highlight the eastern Pacific as a crucial region for determining the zonal SST contrast in response to global warming. Our confidence in a future El Niño-like warming pattern increases considering all local and remote processes investigated in this paper.

Data Availability Statement

All CMIP data are acquired from Earth System Grid Federation (ESGF) node hosted by Lawrence Livermore National Laboratory (LLNL). The authors express special thanks to all of the modeling groups who make CMIP data available. The CMIP data used in this study is available at ESGF data portal (https://esgf-node.llnl.gov/projects/esgf-llnl/). The post-processed data to support the analysis is uploaded in https://doi.org/10.5281/zenodo.5172794.

Acknowledgments
The authors thank the two anonymous reviewers for their constructive comments that improved an earlier version of the paper. CP and SMK were supported by the National Research Foundation of Korea (NRF) grant (NRF-2020R1A2C210150311) funded by the Ministry of Science and ICT (MSIT) of South Korea. MFS was supported by NOAA's Climate Program Office's Modeling, Analysis, Predictions, and Projections (MAPP) program grant NA20OAR4310445. This is IPRC publication 1554 and SOEST contribution 11456. We also wish to thank Jian Lu and Maria Rugenstein for sharing their experiment data, and Yu Kosaka for technical help with CM2.1.

References

Anderson, J. L., Balaji, V., Broccoli, A. J., Cooke, W. F., Delworth, T. L., Dixon, K. W., et al. (2004). The new GFDL global atmosphere and land model AM2-LM2: Evaluation with prescribed SST simulations. *Journal of Climate*, *17*(24), 4641–4673. https://doi.org/10.1175/JCLI-3223.1

Andrews, T., & Webb, M. J. (2018). The dependence of global cloud and lapse rate feedbacks on the spatial structure of tropical pacific warming. *Journal of Climate*, *31*(2), 641–654. https://doi.org/10.1175/JCLI-D-17-0087.1

Armour, K. C., Bitz, C. M., & Roe, G. H. (2013). Time-varying climate sensitivity from regional feedbacks. *Journal of Climate*, *26*(13), 4518–4534. https://doi.org/10.1175/JCLI-D-12-00544.1

Barsugli, J. J., Shin, S. I., & Sardeshmukh, P. D. (2006). Sensitivity of global warming to the pattern of tropical ocean warming. *Climate Dynamics*, *27*(5), 483–492. https://doi.org/10.1007/s00382-006-0143-7

Bayr, T., Dommenget, D., Martin, T., & Power, S. B. (2014). The eastward shift of the Walker circulation in response to global warming and its relationship to ENSO variability. *Climate Dynamics*, *43*(9–10), 2747–2763. https://doi.org/10.1007/s00382-014-2091-y

Bitz, C. M., Gent, P. R., Woodgate, R. A., Holland, M. M., & Lindsay, R. (2006). The influence of sea ice on ocean heat uptake in response to increasing CO_2. *Journal of Climate*, *19*(11), 2437–2450. https://doi.org/10.1175/JCLI3756.1

Burls, N. J., Muir, L., Vincent, E. M., & Fedorov, A. (2017). Extra-tropical origin of equatorial Pacific cold bias in climate models with links to cloud albedo. *Climate Dynamics*, *49*(5–6), 2093–2113. https://doi.org/10.1007/s00382-016-3435-6

Cai, W., Wu, L., Lengaigne, M., Li, T., McGregor, S., Kug, J. S., et al. (2019). Pantropical climate interactions. *Science*, *363*(6430), eaav4236. https://doi.org/10.1126/science.aav4236

Clement, A. C., Seager, R., Cane, M. A., & Zebiak, S. (1996). An ocean dynamical thermostat. *Journal of Climate*, *9*, 2190–2196. https://doi.org/10.1175/1520-0442(1996)009<2190:aodt>2.0.co;2

Delworth, T. L., Broccoli, A. J., Rosati, A., Stouffer, R. J., Balaji, V., Beesley, J. A., et al. (2006). GFDL's CM2 global coupled climate models. Part I: Formulation and simulation characteristics. *Journal of Climate*, *19*(5), 643–674. https://doi.org/10.1175/jcli3629.1

DiNezio, P. N., Clement, A. C., Vecchi, G. A., Soden, B. J., Kirtman, B. P., & Lee, S. K. (2009). Climate response of the equatorial pacific to global warming. *Journal of Climate*, *22*(18), 4873–4892. https://doi.org/10.1175/2009JCLI2982.1

England, M. R., Polvani, L. M., Sun, L., & Deser, C. (2020). Tropical climate responses to projected Arctic and Antarctic sea-ice loss. *Nature Geoscience*, *13*(4), 275–281. https://doi.org/10.1038/s41561-020-0546-9

Fedorov, A. V., Hu, S., Lengaigne, M., & Guilyardi, E. (2015). The impact of westerly wind bursts and ocean initial state on the development, and diversity of El Niño events. *Climate Dynamics*, *44*(5–6), 1381–1401. https://doi.org/10.1007/s00382-014-2126-4

Grose, M. R., Bhend, J., Narsey, S., Gupta, A. S., & Brown, J. R. (2014). Can we constrain CMIP5 rainfall projections in the tropical Pacific based on surface warming patterns? *Journal of Climate*, *27*(24), 9123–9138. https://doi.org/10.1175/JCLI-D-14-00190.1

Heede, U. K., & Fedorov, A. V. (2021). Aerosols and thermostat response to CO_2 increase. *Nature Climate Change*. https://doi.org/10.1038/s41558-021-01101-x

Heede, U. K., Fedorov, A. V., & Burls, N. J. (2020). Time scales and mechanisms for the tropical Pacific response to global warming: A tug of war between the ocean thermostat and weaker walker. *Journal of Climate*, *33*(14), 6101–6118. https://doi.org/10.1175/JCLI-D-19-0690.1

Hwang, Y. T., Xie, S. P., Deser, C., & Kang, S. M. (2017). Connecting tropical climate change with Southern Ocean heat uptake. *Geophysical Research Letters*, *44*(18), 9449–9457. https://doi.org/10.1002/2017GL074972

Kalnay, E., Collins, W., Deaven, D., Gandin, L., Iredell, M., Jenne, R., & Joseph, D. (1996). The NCEP_NCAR 40-year reanalysis project. 1996. pdf. *Bulletin of the American Meteorological Society*, *77*(3), 437–472. https://doi.org/10.1175/1520-0477(1996)077<0437:tnyrp>2.0.co;2

Kang, S. M., Hawcroft, M., Xiang, B., Hwang, Y. T., Cazes, G., Codron, F., et al. (2019). Extratropical–tropical interaction model intercomparison project (ETIN-MIP): Protocol and initial results. *Bulletin of the American Meteorological Society*, *100*(12), 2589–2605. https://doi.org/10.1175/BAMS-D-18-0301.1

Kang, S. M., Xie, S. P., Shin, Y., Kim, H., Hwang, Y. T., Stuecker, M. F., et al. (2020). Walker circulation response to extratropical radiative forcing. *Science Advances*, *6*(47), 1–9. https://doi.org/10.1126/sciadv.abd3021

Kent, C., Chadwick, R., & Rowell, D. P. (2015). Understanding uncertainties in future projections of seasonal tropical precipitation. *Journal of Climate*, *28*(11), 4390–4413. https://doi.org/10.1175/JCLI-D-14-00613.1

Knutson, T. R., & Manabe, S. (1995). Time-mean response over the tropical Pacific to increased CO_2 in a coupled ocean–atmosphere model. *Journal of Climate*, *8*(9), 2181–2199. https://doi.org/10.1175/1520-0442(1995)008<2181:tmrott>2.0.co;2

Kohyama, T., Hartmann, D. L., & Battisti, D. S. (2017). La Niña-like mean-state response to global warming and potential oceanic roles. *Journal of Climate*, *30*(11), 4207–4225. https://doi.org/10.1175/JCLI-D-16-0441.1

Kosaka, Y., & Xie, S. P. (2013). Recent global-warming hiatus tied to equatorial Pacific surface cooling. *Nature*, *501*(7467), 403–407. https://doi.org/10.1038/nature12534

Liu, F., Lu, J., Garuba, O., Leung, L. R., Luo, Y., & Wan, X. (2018). Sensitivity of surface temperature to oceanic forcing via q-flux Green's function experiments. Part I: Linear response function. *Journal of Climate*, *31*(9), 3625–3641. https://doi.org/10.1175/JCLI-D-17-0462.1

Loeb, N. G., Wang, H., Allan, R. P., Andrews, T., Armour, K., Cole, J. N. S., et al. (2020). New generation of climate models track recent unprecedented changes in Earth's radiation budget observed by CERES. *Geophysical Research Letters*, *47*(5), 1–10. https://doi.org/10.1029/2019GL086705

Ma, J., & Xie, S. P. (2013). Regional patterns of sea surface temperature change: A source of uncertainty in future projections of precipitation and atmospheric circulation. *Journal of Climate*, *26*(8), 2482–2501. https://doi.org/10.1175/JCLI-D-12-00283.1

McCreary, J. P., Jr, & Lu, P. (1994). Interaction between the subtropical and equatorial ocean circulations: The subtropical cell. *Journal of Physical Oceanography*, *24*(2), 466–497. https://doi.org/10.1175/1520-0485(1994)024,0466:IBTSAE.2.0.CO;2

Mechoso, C. R., Losada, T., Koseki, S., Mohino-Harris, E., Keenlyside, N., Castaño-Tierno, A., et al. (2016). Can reducing the incoming energy flux over the Southern Ocean in a CGCM improve its simulation of tropical climate? *Geophysical Research Letters*, *43*(20), 11057–11063. https://doi.org/10.1002/2016GL071150

Meehl, G. A., & Washington, W. M. (1996). El Niño-like climate change in a model with increased atmospheric CO_2 concentrations. *Nature*, *382*(July), 56–60. https://doi.org/10.1038/382056a0

Neale, R. B., Richter, J., Park, S., Lauritzen, P. H., Vavrus, S. J., Rasch, P. J., & Zhang, M. (2013). The mean climate of the community atmosphere model (CAM4) in forced SST and fully coupled experiments. *Journal of Climate*, *26*(14), 5150–5168. https://doi.org/10.1175/JCLI-D-12-00236.1

Ramanathan, V., & Collins, W. (1991). Thermodynamic regulation of ocean warming by cirrus clouds deduced from observations of the 1987 El Niño. *Nature*, *351*(6321), 27–32. https://doi.org/10.1038/351027a0

Rugenstein, M., Bloch-Johnson, J., Abe-Ouchi, A., Andrews, T., Beyerle, U., Cao, L., et al. (2019). Longrunmip motivation and design for a large collection of millennial-length AOGCM simulations. *Bulletin of the American Meteorological Society*, *100*(12), 2551–2569. https://doi.org/10.1175/BAMS-D-19-0068.1

Seager, R., Cane, M., Henderson, N., Lee, D. E., Abernathey, R., & Zhang, H. (2019). Strengthening tropical Pacific zonal sea surface temperature gradient consistent with rising greenhouse gases. *Nature Climate Change*, *9*(7), 517–522. https://doi.org/10.1038/s41558-019-0505-x

Senior, C. A., & Mitchell, J. F. B. (2000). The time-dependence of climate sensitivity. *Geophysical Research Letters*, *27*(17), 2685–2688. https://doi.org/10.1029/2000GL011373

Stuecker, M. F. (2021). New insights into future tropical climate change. *Nature Climate Change*, *11*, 645–646. https://doi.org/10.1038/s41558-021-01107-5

Stuecker, M. F., Timmermann, A., Jin, F. F., Proistosescu, C., Kang, S. M., Kim, D., et al. (2020). Strong remote control of future equatorial warming by off-equatorial forcing. *Nature Climate Change*, *10*(2), 124–129. https://doi.org/10.1038/s41558-019-0667-6

Thomas, M. D., & Fedorov, A. V. (2017). The eastern subtropical pacific origin of the equatorial cold bias in climate models: A Lagrangian perspective. *Journal of Climate*, *30*(15), 5885–5900. https://doi.org/10.1175/JCLI-D-16-0819.1

Trenberth, K. E., Branstator, G. W., Karoly, D., Kumar, A., Lau, N. C., & Ropelewski, C. (1998). Progress during TOGA in understanding and modeling global teleconnections associated with tropical sea surface temperatures. *Journal of Geophysical Research*, *103*(C7), 14291–14324. https://doi.org/10.1029/97jc01444

Webb, M. J., Senior, C. A., Sexton, D. M. H., Ingram, W. J., Williams, K. D., Ringer, M. A., et al. (2006). On the contribution of local feedback mechanisms to the range of climate sensitivity in two GCM ensembles. *Climate Dynamics*, *27*(1), 17–38. https://doi.org/10.1007/s00382-006-0111-2

Xie, S. P., Deser, C., Vecchi, G. A., Ma, J., Teng, H., & Wittenberg, A. T. (2010). Global warming pattern formation: Sea surface temperature and rainfall. *Journal of Climate*, *23*(4), 966–986. https://doi.org/10.1175/2009JCLI3329.1

Yun, K. S., Timmermann, A., & Stuecker, M. (2021). Synchronized spatial shifts of Hadley and Walker circulations. *Earth System Dynamics*, *12*(1), 121–132. https://doi.org/10.5194/esd-12-121-2021

Zhang, L., & Li, T. (2014). A simple analytical model for understanding the formation of sea surface temperature patterns under global warming. *Journal of Climate*, *27*(22), 8413–8421. https://doi.org/10.1175/JCLI-D-14-00346.1

Zhang, X., Deser, C., & Sun, L. (2021). Is there a tropical response to recent observed Southern Ocean cooling? *Geophysical Research Letters*, *48*(5), e2020GL091235. https://doi.org/10.1029/2020GL091235

Zhou, C., Zelinka, M. D., & Klein, S. A. (2017). Analyzing the dependence of global cloud feedback on the spatial pattern of sea surface temperature change with a Green's function approach. *Journal of Advances in Modeling Earth Systems*, *9*(5), 2174–2189. https://doi.org/10.1002/2017MS001096

Reference From the Supporting Information

Jia, F., & Wu, L. (2013). A study of response of the equatorial pacific SST to doubled-CO2 forcing in the coupled CAM-1.5-layer reduced-gravity ocean model. *Journal of Physical Oceanography*, *43*(7), 1288–1300. https://doi.org/10.1175/JPO-D-12-0144.1